

Orbital ordering in the manganites: Resonant x-ray scattering predictions at the manganese L_{II} and L_{III} edges

C. W. M. Castleton*

European Synchrotron Radiation Facility, BP 220, F-38043 Grenoble Cédex, France

M. Altarelli

*Sincrotrone Trieste, Area Science Park, 34012 Basovizza, Trieste, Italy**and Abdus Salam International Centre for Theoretical Physics, Strada Costiera 11, 34014 Trieste, Italy*

(Received 29 November 1999; revised manuscript received 16 February 2000)

It is proposed that the observation of orbital ordering in manganite materials should be possible at the L_{II} and L_{III} edges of manganese using x-ray resonant scattering. If performed, dipole selection rules would make the measurements much more direct than the disputed observations at the manganese K edge. They would yield specific information about the type and mechanism of the ordering not available at the K edge, as well as permitting the effects of orbital ordering and Jahn-Teller ordering to be detected and distinguished from one another. Predictions are presented based on atomic multiplet calculations, indicating distinctive dependence on energy, as well as on polarization and on the azimuthal angle around the scattering vector.

I. INTRODUCTION

The manganite materials, such as $\text{La}_{1-x}\text{Sr}_x\text{MnO}_3$ and $\text{La}_{1-x}\text{Sr}_{1+x}\text{MnO}_4$, have received much attention recently, due to the complex interplay of electronic, spin and orbital degrees of freedom which they exhibit. This includes observation of colossal magnetoresistance and a large variety of phase transitions as a function of temperature, magnetic field, and doping. Among the most interesting of late have been the charge and orbitally ordered states observed in a variety of materials such as $\text{La}_{0.5}\text{Sr}_{1.5}\text{MnO}_4$,^{1,2} LaMnO_3 ,³ $\text{La}_{0.5}\text{Ca}_{0.5}\text{MnO}_3$,⁴ (see also Refs. 5 and 6), $\text{La}_{0.33}\text{Ca}_{0.67}\text{MnO}_3$,⁷ and $\text{La}_{0.25}\text{Ca}_{0.75}\text{MnO}_3$.⁸ As the temperature is lowered all of the materials (except for the undoped LaMnO_3) show a charge ordering transition in which separate sublattices develop for Mn^{3+} and Mn^{4+} ions. An orbital ordering transition on the Mn^{3+} sublattice (all Mn sites in the case of LaMnO_3) is then believed to occur, followed at (generally) lower temperatures by a magnetic ordering transition. The structure of all of these orbitally ordered states is believed to be very similar, and our results will be relevant to all. The exception will be LaMnO_3 , for which the period of the orbital order is too small, (see later). For simplicity we will refer mostly to the layered material, $\text{La}_{0.5}\text{Sr}_{1.5}\text{MnO}_4$, returning to the others at the end.

In the case of $\text{La}_{0.5}\text{Sr}_{1.5}\text{MnO}_4$ the charge ordering transition is at about $T_{\text{CO}}=220$ K, with a unit variation of valence observed between the sublattices.^{1,2} This results in a doubling of the unit cell and the appearance of forbidden reflections at, for example, $(\frac{1}{2}, \frac{1}{2}, 0)$. At about $T_N=160$ K, as seen by neutron scattering,¹ a complex antiferromagnetic ordering occurs, involving both manganese sublattices. (See Fig. 1.) However, the antiferromagnetic transition observed in the magnetic susceptibility⁹ is higher, concurrent with the charge ordering. It seems likely, therefore, that in-plane antiferromagnetic order develops at a temperature $T_{N(ab)}=220$ K and becomes fully three dimensional at $T_{N(c)}$

=160 K. (Rod-like neutron scattering has been reported between T_N and T_{CO} .¹)

At the Mn^{3+} sites the Hund's rule coupling is strong, and the crystal field has a large cubic (O_h) component. Described at one electron level, the $\text{Mn}^{3+} 3d^4$ configuration thus becomes a twofold degenerate $t_{2g}^3 e_g^1$ configuration. (See Fig. 2.) This degeneracy can be lifted, with (in principle) an associated Jahn-Teller (JT) distortion of the oxygen octahedron, reducing the symmetry to D_{4h} . Hence we shall denote the two components of the e_g level as $3d_{3z^2-r^2}$ and $3d_{x^2-y^2}$. Goodenough¹⁰ showed that the spin

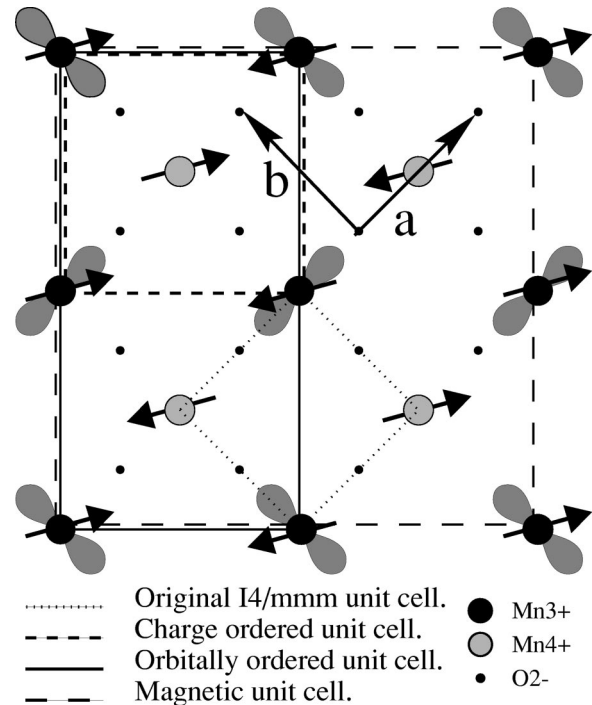


FIG. 1. Charge, orbital, and spin ordering in the MnO_2 planes of $\text{La}_{0.5}\text{Sr}_{1.5}\text{MnO}_4$.

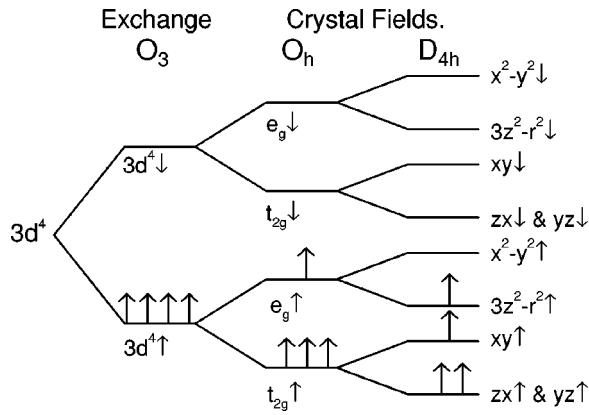


FIG. 2. Schematic one-electron energy level diagram for the $3d$ shell of Mn^{3+} in a tetragonally distorted oxygen octahedron.

ordering is actually dependant upon the ordering of this orbital degree of freedom. Above T_{CO} all Mn sites have $3d_{3z^2-r^2\uparrow}$ (part) filled, oriented along the crystal c axis with a macroscopic tetragonal distortion. Below $T_{N(c)}$, however, a distinctive ‘‘herring-bone’’ pattern is required in order to explain the observed spin structure, as shown in Fig. 1. This orbital pattern again doubles the unit cell, having the wavevector $(\frac{1}{4}, \frac{1}{4}, 0)$. This is claimed to have been observed recently using resonant x-ray scattering at the Mn K edge.² These results indicate that orbital order develops at the same temperature as the charge ordering: $T_{\text{OO}} = T_{\text{CO}} (= T_{N(ab)}) = 220$ K. The fact that the spins do not order out of plane until a lower temperature $T_{N(c)}$ is not in disagreement with this, since for $\text{La}_{0.5}\text{Sr}_{1.5}\text{MnO}_4$ Goodenough’s orbitally mediated spin interactions only produce couplings in the ab plane, not up the c axis. This leaves us with at least two possible mechanisms for the orbital ordering—it could be due to the spin ordering it permits, or to the JT distortions, or to a combination of the two. The question of which mechanism is the more important is still disputed. In other materials (such as¹¹ LaMnO_3 and⁴ $\text{La}_{0.5}\text{Ca}_{0.5}\text{MnO}_3$) the ordering of the JT distortions around the Mn^{3+} sites has been observed directly, using high resolution neutron and x-ray diffraction, and crystallographic refinement. The level of distortions appears to vary somewhat, from about 7% to 12%, suggesting that the JT mechanism may at least be not the sole mechanism of importance. Indeed, in $\text{La}_{0.5}\text{Sr}_{1.5}\text{MnO}_4$ only a 1% oxygen breathing mode has so far been observed,¹ although detailed crystallographic refinement is not reported. It could thus be suggested² that here the JT distortions actually remain along the c axis even when the orbitals have ordered in the ab plane, and that the only mechanism of importance for this material is the Goodenough spin ordering mechanism. The complete absence of accompanying JT distortion ordering in the ab plane seems very unlikely, however. More detailed crystallographic refinement might be able to clarify this, as was the case^{4,12} for $\text{La}_{0.5}\text{Ca}_{0.5}\text{MnO}_3$.

What is clear is that the interaction and interdependence of the spin, orbital and JT ordering is complex, and not yet fully understood. In order to approach a better understanding it would be very helpful to be able to observe the JT and orbital ordering independently of one another. The K edge experiments so far performed fail to do this. They are indirect, in the sense that they probe primarily the $4p$ shell,

rather than the $3d$ shell in which the supposedly ordered orbitals lie. The sensitivity was thought to have arisen from a mixture of the Coulomb interaction with the ordered $3d$ electrons and the JT distortion of the site.¹⁵ It has since been shown^{13,14} that the experiment is about 100 times more sensitive to the accompanying JT ordering than to the orbital ordering. Although an interference term between the two¹⁴ does leave the possibility of distinguishing them by looking at the energy dependence of the peak, it seems rather doubtful that a direct observation of orbital ordering, as distinct from JT ordering, is possible at the Mn K edge. Since the orbital believed to order is the $\text{Mn}^{3+} 3d_{3z^2-r^2\uparrow}$, it seems logical to try resonant scattering at the Mn L_{II} and L_{III} edges, probing the $3d$ shell itself. Unfortunately these edges lie in the soft x-ray region, so, although the Bragg angle for the $(\frac{1}{4}, \frac{1}{4}, 0)$ reflection is real (62.9° at the L_{III} edge), the penetration depth will be very short. This will make the experiment surface sensitive and rather difficult, but not necessarily impossible. It is certainly the correct way to proceed if one wishes to directly probe the orbital order in these materials.

In the next section we will discuss the origin of the scattering and its azimuthal and polarization dependence. In Sec. III we perform crystal field multiplet calculations to examine the energy dependence of the scattering and we discuss the distinct effects of orbital and JT ordering. Conclusions are presented in Sec. IV.

II. POLARIZATION AND AZIMUTHAL ANGLE DEPENDENCE

In contrast to the K edge experiment, interpretation of the $L_{\text{II(III)}}$ edge experiment, where a $2p$ electron is promoted directly into the $3d$ shell, is very clear. At one electron level, if the $3d_{3z^2-r^2\uparrow}$ orbital is filled (see Fig. 2), the edge itself consists of the transition $2p \rightarrow 3d_{x^2-y^2\uparrow}$. This will clearly have a very different amplitude if the incoming photon is polarized parallel rather than perpendicular to the local ‘‘ z ’’ direction (\hat{z}) of the ion. This local z direction alternates along the $(1, 1, 0)$ direction between the a and b axes of the crystal, with periodicity $2\sqrt{2}$ (relative to the original unit cell). For light polarized in the ab plane one therefore anticipates seeing the $(\frac{1}{4}, \frac{1}{4}, 0)$ forbidden reflection, the amplitude being proportional to the difference between the scattering amplitude for a Mn^{3+} ion with its local z direction parallel to the crystal a axis and the scattering amplitude for one with its local z parallel to b . This is, of course, the same as the difference between the amplitudes for light polarized parallel and perpendicular to the z direction of an individual ion. Light polarized parallel to the crystal c axis, however, is perpendicular to the local z directions of all the Mn^{3+} ions, so the scattering factor is the same at each site, and the scattering must be zero. This leads to a complex dependence on polarization and on the azimuthal angle around the scattering vector.

More rigorously, the scattering can be viewed as originating in the 3rd term of the single ion $E1$ resonant scattering amplitude given by Hannon *et al.*,¹⁶

$$f_{\text{ion}}^{E1} = (\boldsymbol{\epsilon}^* \cdot \hat{\mathbf{z}})(\boldsymbol{\epsilon}^0 \cdot \hat{\mathbf{z}})(2F_{1,0}^{(e)} - F_{1,1}^{(e)} - F_{1,-1}^{(e)}), \quad (1)$$

where $F_{1,q}$ are the spherical components of the transition amplitude and $\boldsymbol{\epsilon}^0(\boldsymbol{\epsilon}^f)$ the polarization vector for the incoming (outgoing) beam. The scattering amplitude at the $(\frac{1}{4}, \frac{1}{4}, 0)$ reflection is given by the difference between f_{ion}^{E1} for two Mn^{3+} ions with $\hat{\mathbf{z}}$ equal to $\hat{\mathbf{a}}$ and $\hat{\mathbf{b}}$. (Unit vectors along a and b respectively.) Hence

$$f^{E1} = \begin{bmatrix} (\boldsymbol{\epsilon}^{f*} \cdot \hat{\mathbf{a}})(\boldsymbol{\epsilon}^0 \cdot \hat{\mathbf{a}}) \\ -(\boldsymbol{\epsilon}^{f*} \cdot \hat{\mathbf{b}})(\boldsymbol{\epsilon}^0 \cdot \hat{\mathbf{b}}) \end{bmatrix} (2F_{1,0}^{(e)} - F_{1,1}^{(e)} - F_{1,-1}^{(e)}). \quad (2)$$

The polarization dependence, being purely geometric, is the same as that previously observed at the K edge.^{2,3} Resolving $\boldsymbol{\epsilon}$ into σ and π components, and performing two rotations [first through the azimuthal angle ϕ , second through $\pi/4$ around $\hat{\mathbf{c}}$, since the wave vector is along $(1, 1, 0)$ but the orbitals alternate between $(1, 0, 0)$ and $(0, 1, 0)$] we can express the polarization in terms of the crystal coordinates. It is then straightforward to show that $\sigma^0 \rightarrow \sigma^f$ and $\pi^0 \rightarrow \pi^f$ scattering is forbidden. For the $\sigma^0 \rightarrow \pi^f$ and $\pi^0 \rightarrow \sigma^f$ channels the scattering intensity turns out to be

$$I(\theta, \phi) = \cos^2 \theta \sin^2 \phi (2F_{1,0}^{(e)} - F_{1,1}^{(e)} - F_{1,-1}^{(e)})^2, \quad (3)$$

where 2θ is the scattering angle, and ϕ the azimuthal angle around the scattering vector.

More interesting is the energy dependence. From the naive description above it is intuitively clear that there must be at least one energy range where $I(0, \pi/2) \neq 0$, since $3d_{3z^2-r^2\uparrow}$ is filled and $3d_{x^2-y^2\uparrow}$ is empty. Indeed, one expects there to be scattering in a second, higher energy, as the presence of an electron in the $3d_{3z^2-r^2\uparrow}$ orbital will split the $3d_{3z^2-r^2\downarrow}$ and $3d_{x^2-y^2\downarrow}$ orbitals by the Coulomb interaction. This will happen even in the absence of any JT distortion. This is because the Coulomb interaction between two electrons occupying orbitals with the same spatial distribution should be much larger than that between electrons in orbitals with different spatial distributions. If the latter Coulomb interactions are neglected, then, at one electron level, we should not expect any splitting in the $t_{2g\downarrow}$ level, unless it comes from Jahn-Teller effects. We therefore also anticipate some differences between the case of orbital ordering alone, and that of combined orbital and JT ordering. As discussed above, the latter case is the most likely, so we would here anticipate three main peaks at both the L_{II} and L_{III} edges.

These arguments tell us nothing about the relative size or spacing between the peaks, or of the possibility of smaller peaks being obscured by larger ones. So, to be more concrete, and to have a more detailed idea of the energy dependence that can be expected for $I(0, \pi/2)$, we have performed an atomic multiplet calculation for Mn^{3+} in a D_{4h} crystal field, using the Cowan multiplet codes and the ‘‘Racah’’ crystal field program of B. Searle. There being no clear set of crystal field parameters in the literature we first performed a fit to the soft-XAS spectrum for LaMnO_3 .¹⁷ The atomic environment of the Mn^{3+} ions in LaMnO_3 is similar in coordination and symmetry to that in our case.

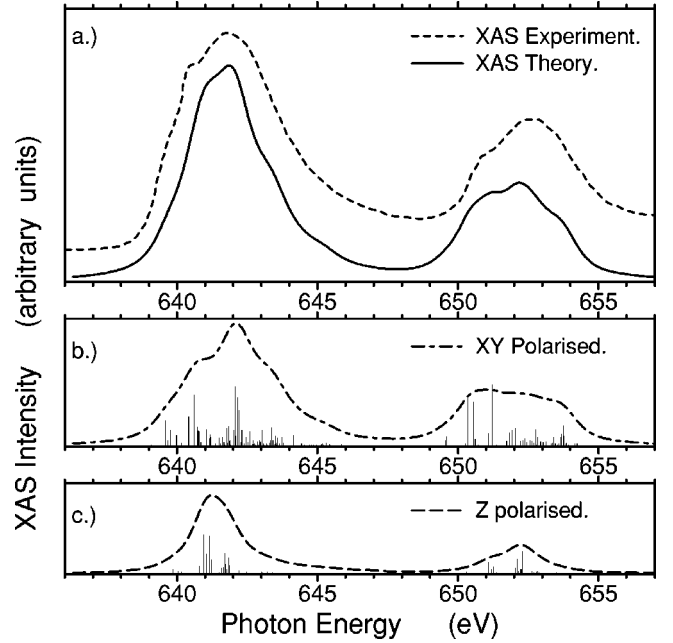


FIG. 3. Soft-XAS spectrum for Mn^{3+} in LaMnO_3 . (a) Experiment (taken from Ref. 17) and D_{4h} crystal field multiplet calculation. (b) xy and (c) z polarized contributions.

III. CRYSTAL FIELD MULTIPLY CALCULATIONS AND ENERGY DEPENDENCE

A. Fit to the XAS spectrum of LaMnO_3

Our fit to the soft-XAS spectrum is shown in Fig. 3(a). Hartree-Fock values for the Slater integrals are scaled to 65%, and crystal fields parameters are $X^{400}=3.42$, $X^{420}=-4.05$ and $X^{220}=-2.34$, where 420, etc. are the relevant branchings for the crystal field group chain $O_3 \rightarrow O_h \rightarrow D_{4h}$, in Racah notation. (This corresponds to $D_q=0.25$, $D_s=0.28$, $D_t=0.25$ in standard notation.) The scaling of the Hartree-Fock parameters is strong, but this is in keeping with the findings of previous related studies.^{18,17} Note also that the line of parameters $D_s=0.55-D_q$, $D_t=2D_q-0.25$, $D_q=0.15 \rightarrow 0.25$, with 60% \rightarrow 70% scaling, produces very similar results.

Using D_{4h} symmetry we find good agreement with the experiment, in contrast to Abbate *et al.*¹⁷ who got only a rough fit using O_h symmetry. There remain, however, a few features of the spectra that do not quite match. These should be due partly to the presence of ligand holes, (absent in our calculation) and partly to the neglect of the inequivalence between the x and y directions. (Each Mn^{3+} has one of these in the crystal’s ab plane, the other along the c axis.) This would reduce D_{4h} to D_{2h} , with an additional splitting between $3d_{xz}$ and $3d_{zy}$, and alterations to others.

It is also the case that there is an anisotropy at the Mn^{4+} sites, since each Mn^{4+} has two filled Mn^{3+} $3d_{3z^2-r^2}$ orbitals pointing towards it, set 90° apart, and two empty. (See Fig. 1.) This breaks the inversion symmetry and is modulated with the same wave vector as the orbital ordering itself. However, the Mn^{3+} $3d_{3z^2-r^2}$ lie the other side of the intervening oxygen sites, so the effect should be tiny compared to that on the Mn^{3+} sites. It should also occur at a slightly

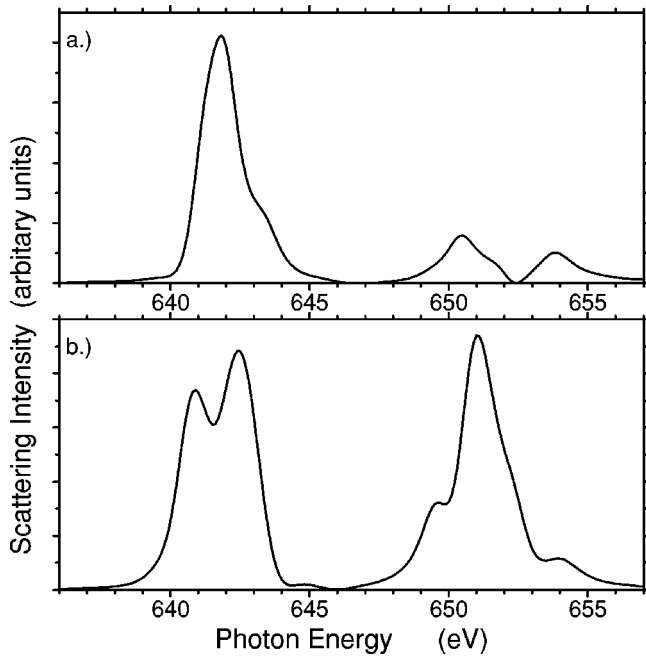


FIG. 4. (a) Calculated intensity at the Mn $L_{II(III)}$ edges. (b) Calculated intensity with signs of X^{420} and X^{220} reversed.

different energy. We are therefore confident that any effect seen in this experiment would be arising from the orderings on the Mn^{3+} sublattice itself.

In Figs. 3(b) and 3(c) we include the XAS contributions from x rays polarized in the xy plane and along the z axis. Although the one-electron picture is blurred out by the multiplet interactions it is still possible to discern about 4 broad levels, most clearly at the L_{III} edge. The 1st and 4th are polarized mostly in the xy plane, the 2nd largely parallel to the z axis, but with significant xy contributions also. The 3rd is again mixed, but predominantly xy . The first band can be reasonably identified as the $3d_{x^2-y^2\uparrow}$ level, albeit rather broadened and with other contributions mixed in. The others can probably be labeled, at one electron level, according to the scheme in Fig. 2, provided the $3d_{xy\downarrow}$ and $3d_{3z^2-r^2\downarrow}$ are sufficiently broadened and shifted that they overlap completely. Hence, the 2nd level comprises mostly the $3d_{xz\downarrow}$ and $3d_{zy\downarrow}$ of the split $t_{2g\downarrow}$ level, and the 3rd the $3d_{xy\downarrow}$ component, overlapping with the $3d_{3z^2-r^2\downarrow}$ from the $e_{g\downarrow}$. Finally, the 4th level would be from transitions to the $3d_{3x^2-y^2\downarrow}$ orbital.

B. Resonant x-ray scattering

Turning to the resonant scattering, we plot in Fig. 4(a) the maximum scattering intensity, $I(0,\pi/2)$. We see that there is a distinct structure as a function of energy. Comparing the energy scale with that of Fig. 3 we note also that the greatest intensity does not come from transitions to the empty $3d_{x^2-y^2\uparrow}$ orbital itself, but, from transitions to the split $t_{2g\downarrow}$ levels, just above. This strong scattering peak occurs only at the L_{III} edge. On its high energy side we see a shoulder, but any shoulder to the low energy side is too small to be noticeable. At the L_{II} edge we see two main peaks, with a shoulder on the high energy side of the lower one. The nature of these other peaks and shoulders will be discussed later.

The energy dependence of $I(0,\pi/2)$ carries specific information about the environment of the Mn^{3+} sites, helping us answer questions to do with the type and origin of the ordering, as discussed previously. For example, in the K edge experiments it was not possible² to differentiate between the $3d_{3x^2-r^2}/3d_{3y^2-r^2}$ orbital ordering actually believed to occur and the alternative $3d_{x^2-z^2}/3d_{z^2-y^2}$ ordering. However, at the L edges the two should have very different energy dependences. To illustrate this point, we have recalculated the $L_{II(III)}$ edge scattering, keeping the same crystal field magnitudes as before, but reversing the sign of the D_{4h} terms X^{420} and X^{220} . This makes $3d_{x^2-y^2}$ the occupied orbital, mimicking the alternative $3d_{x^2-z^2}/3d_{z^2-y^2}$ ordering. The result is shown in Fig. 4(b), and is clearly distinguishable from Fig. 4(a). We emphasize, however, that this curve is not intended as a specific prediction, since it is not derived from any experimental spectra for a Mn^{3+} ion with the $3d_{x^2-y^2\uparrow}$ orbital filled. It is intended just as an illustration that much more information should be available at the L edges than at the K edge. Extraction of such information would require detailed fits to actual experimental data, when such exist.

C. Distinguishing orbital order and Jahn-Teller order

It should also be possible to differentiate between the scattering due to orbital ordering alone and that due to combined orbital and JT distortion ordering, helping us tackle the question of which mechanism is the more important. Within the confines of the multiplet codes we need to keep X^{420} and X^{220} nonzero in order to make $3d_{3z^2-r^2\uparrow}$ the occupied orbital. This means that so far we have actually included the JT effects as well, implicitly assuming the involvement of that mechanism. We would now like to identify which parts of the predicted spectrum, if any, come from the JT ordering, and which come from orbital ordering alone. To do this, we note first that whilst X^{420} and X^{220} must remain nonzero, in order to split $3d_{3z^2-r^2}$ and $3d_{x^2-y^2}$ and observe orbital ordering at all, the actual size of the splitting required is not important, down to some limit set by truncation within the code. Thus we can choose a very small tetragonal distortion in order to select the $3d_{3z^2-r^2}$ orbital in the initial state, and then use scaling arguments to differentiate between the orbital ordering effects and the residual JT effects. Hence we can scale X^{420} and X^{220} by some $\delta \rightarrow 0$, progressively removing the effects of the JT distortions, whilst keeping the scattering from the ordered orbitals. (Note that δ is not intended as an experimental fitting parameter, it is simply a tool to ‘switch off’ the JT distortion, leaving pure orbital ordering, so that we can separate out the two contributions.)

In Fig. 5 we show the scattering for a few values of δ . (The ratio X^{420}/X^{220} is kept constant.) For $\delta < 0.25$ the JT effects are small and we are essentially left with the effect of the orbital ordering alone. In Fig. 6 we plot the heights of the four main peaks against δ . It is clear that there is only one significant peak due directly to the JT distortion. It is labeled with a square symbol on Fig. 5, and lies in the L_{III} edge. This is the peak corresponding earlier to transitions into the split $t_{2g\downarrow}$ levels. In Fig. 6 the peak height scales to a very small value as $\delta \rightarrow 0.0$, indicating an OO contribution of only about 4%. A better estimate might have come from scaling the weight under the peak, but this is complicated by the pres-

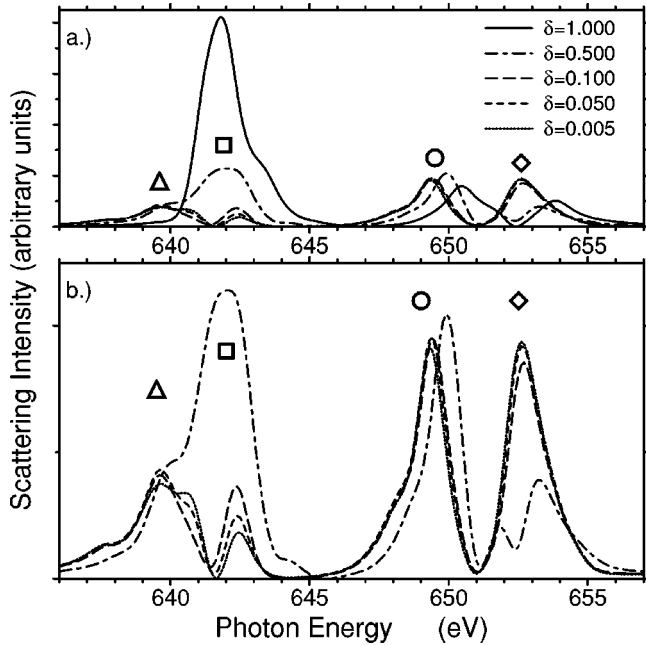


FIG. 5. (a) Scattering with D_{4h} contributions reduced by δ . Symbols label the peaks scaled with δ in Fig. 6. (b) Peak detail at lower δ values.

ence of the shoulder. Comparing the weight under this peak in the $\delta=0.005$ and $\delta=1.000$ curves, an OO contribution of around 1.3–1.7% is obtained, depending on where one cuts the shoulder. That this peak should be due essentially to the JT distortions rather than the presence of the ordered e_g electron is in complete agreement with our previous one electron level arguments. The equivalent peak at the L_{II} edge is the shoulder on the lower main peak. The δ dependence of its energy is different from that of the two main peaks at this edge, however, so it is visible as a separate peak in the $\delta=0.5$ curve. At smaller δ it is too small to be distinguishable. The difference between this peak and the equivalent peak at the L_{III} edges is due to the core hole potential; this we have verified by repeating the calculation with the core hole potential absent.

The three other peaks are due principally to the ordered orbital occupancy, as their heights do not diminish with di-

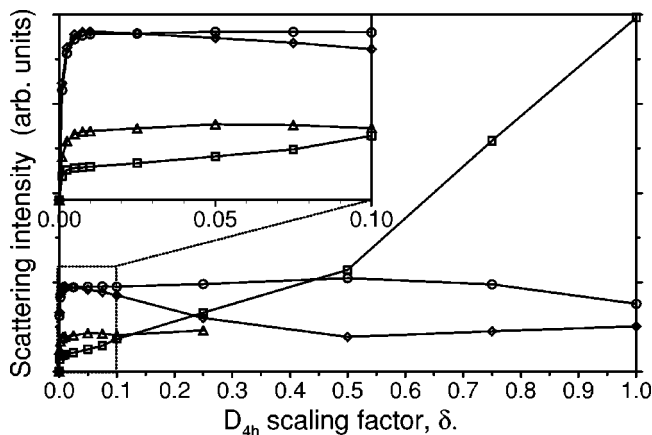


FIG. 6. Heights of the peaks labeled by symbols in Fig. 5, plotted against the scaling parameter δ . Inset gives $\delta=0.0 \rightarrow 0.1$.

minishing δ . Indeed, the heights are stable over about two orders of magnitude, and scale to nonzero values as the JT distortions go to zero. (Their collapse to zero for very small δ is an artifact of numerical truncation in the calculation.) The most interesting of these is the peak labeled with a circle at the L_{II} edge. Comparison with the peak identifications in Fig. 3 (see previous section) shows that this is due to resonant transitions into the unoccupied $3d_{x^2-y^2\uparrow}$, so we would expect to see it even in the complete absence of JT distortions. Estimating the size of the JT contribution from the δ scaling of the peak height is difficult, but suggests a negative contribution of around 8–20%. It is equally difficult to use scaling of the weight under the curve, as there is again a shoulder. Depending on where we cut the shoulder we get estimates in the 10–30% range. It can also be seen clearly that the location of the peak shifts downwards in energy by 1.06 eV. The equivalent peak at the L_{III} edge moves even further, being invisible for $\delta=1.000$, hidden under the square labeled peak. At first glance this movement might suggest that the contributions from JT ordering are much larger, but this is not the case. At one electron level (see Fig. 2) we see that, even in the absence of any JT distortion, this peak should exist as soon as the $3d_{3z^2-r^2\uparrow}$ orbital is occupied and ordered. Any JT distortion on top of this will not add or take anything at all from the scattering intensity, but it will move the $3d_{x^2-y^2\uparrow}$ level upwards in energy, and hence also the scattering. This is indeed what we see in Fig. 5. The changes in peak height and weight come only when multiplet contributions beyond one electron level are included. Hence, the location of this peak in energy is controlled partly by OO and partly by JT ordering, but its existence and weight are still essentially due to the OO itself.

The other two peaks arise from the splitting of the $e_{g\downarrow}$ levels. At the L_{II} edge this peak (labeled with a diamond) moves downwards as the JT distortions are switched off, and actually grows. The equivalent peak at the L_{III} edge is not labeled, as it is weaker, and moves from being a shoulder on the square labeled peak at $\delta=1.000$ to being a shoulder on the triangle labeled peak at $\delta=0.050$ and below. The diamond labeled peak actually grows by almost a factor of two as the JT distortions are removed. This is again understandable at one electron level. As we noted earlier, in the absence of any distortion, we would expect the $3d_{3z^2-r^2\downarrow}$ orbital to lie above the $3d_{x^2-y^2\downarrow}$ orbital due Coulomb interaction with the occupied $3d_{3z^2-r^2\uparrow}$. However, in the absence of the Coulomb interaction, but with the JT distortion elongating the ion along the z axis, we would expect $3d_{3z^2-r^2\downarrow}$ to lie below $3d_{x^2-y^2\downarrow}$. Hence for the diamond labeled peak the two contributions are in competition. Apparently the JT dominates at $\delta=1.000$, since Fig. 3 indicates that $3d_{3z^2-r^2\downarrow}$ lies below $3d_{x^2-y^2\downarrow}$. In Figure 6 we see a minimum in the peak height around $\delta=0.500$, where the two contributions balance (multiplet broadening prevents the peak disappearing completely). Below this OO dominates, and the peak intensity grows.

The prediction from the δ scaling is that the scattering shown in Fig. 4(a) is dominated at the L_{III} edge by JT ordering, although orbital order leads to a clear shoulder to the high energy side of the main JT peak. At the L_{II} edge, on the other hand, whilst the scattering is predicted to be rather weaker, it is dominated heavily at the lower end by the or-

orbital ordering. Observation of scattering intensity here would thus be a reasonably good measurement of orbital order, independent of the presence or absence of JT order. Confirmation of this could again be sought by more detailed fitting to experimental data, were the measurement to be actually performed. [We anticipate some difference between experimental data and that shown in Fig. 4(a) since our calculation is based upon a fit to the XAS spectrum for Mn^{3+} in a slightly different setting.]

D. Orbital ordering in other materials

Returning now to the other manganite materials, we note that, for example, $\text{La}_{0.5}\text{Ca}_{0.5}\text{MnO}_3$ shows exactly the same charge and orbital ordering in the ab plane,⁴ leading to the same energy, polarization and azimuthal dependence as for the layered material. The unit cell is normally indexed differently, so that the fundamental wave vector is $(\frac{1}{2}, 0, 0)$, but this again gives a period of about 10.9 Å, or an angle of 62.9° at the Mn L_{III} edge. Similarly for $\text{La}_{0.33}\text{Ca}_{0.67}\text{MnO}_3$, orbital order has been reported⁷ with a wave vector of $(\frac{1}{3}, 0, 0)$, giving a period around 16.2 Å. The structure is slightly different, but the Mn^{3+} local z directions alternate between $(1, 1, 0)$ and $(1, -1, 0)$, still giving the same energy, polarization and azimuthal dependence. In practice, we expect that this technique, if realized, could measure and differentiate between both JT and orbital ordering in a wide variety of manganite materials. The exception, unfortunately, is LaMnO_3 itself. Here, in the absence of Mn^{4+} ions, the period of the orbital order is only about 5.4 Å, too short for the Mn $L_{\text{II(III)}}$ edges. The minimum orbital order period for which a reflection could exist at the Mn L_{III} edge is about 9.7 Å.

IV. CONCLUSION

We have demonstrated that, in principle, it should be possible to make direct observations of orbital ordering as well as Jahn-Teller ordering in many of the manganite materials, using resonant x-ray scattering at the Mn $L_{\text{II(III)}}$ edges. This is likely to be true also of resonant L edge scattering in other materials which combine orbital ordering with charge ordering. For the current case of the manganites, we have shown that sensitivity at the L_{III} edge should be primarily to the accompanying Jahn-Teller ordering, whilst that at the L_{II} edge should be due to the orbital ordering itself. The intensity would have specific energy and polarization dependences, and a \sin^2 dependence on the azimuthal angle around the scattering vector. The measurement would be theoretically much more direct than the disputed resonant x-ray scattering measurements so far performed at the Mn K edge, because dipole selection rules allow scattering directly from the ordered orbitals themselves, rather than from some other unoccupied orbitals, strongly hybridised with surrounding oxygen orbitals, higher up in energy. With the aid of suitable fitting of the energy dependence, the measurement would provide much more detailed information, particularly about the type of ordering present, the orbitals actually involved and the relative importance of the possible ordering mechanisms.

ACKNOWLEDGMENTS

C.W.M.C. would like to thank P. Carra for helpful discussions and assistance in learning to use the Cowan and Racah codes. He also thanks E. Pellegrin, T. Forgan, F. de Bergevin, and P. Abbamonte for helpful discussions.

*Present address: Dept. of Physics, University of Uppsala, P.O. Box 530, SE-75121 Uppsala, Sweden.

¹B.J. Sternleib, J.P. Hill, U.C. Wildgruber, G.M. Luke, B. Nachumi, Y. Moritomo, and Y. Tokura, Phys. Rev. Lett. **76**, 2169 (1996).

²Y. Murakami, H. Kawada, H. Kawata, M. Tanaka, T. Arima, Y. Moritomo, and Y. Tokura, Phys. Rev. Lett. **80**, 1932 (1998).

³Y. Murakami, J.P. Hill, D. Gibbs, M. Blume, I. Koyama, M. Tanaka, H. Kawata, T. Arima, Y. Tokura, K. Hirota, and Y. Endoh, Phys. Rev. Lett. **81**, 582 (1998).

⁴P.G. Radaelli, D.E. Cox, M. Marezio, and S-W. Cheong, Phys. Rev. B **55**, 3015 (1997).

⁵T. Vogt, A.K. Cheetham, R. Mahendiran, A.K. Raychaudhuri, R. Mahesh, and C.N.R. Rao, Phys. Rev. B **54**, 15303 (1996).

⁶M. von Zimmermann, J.P. Hill, M. Blume, D. Casa, B. Keimer, Y. Murakami, Y. Tomioka, and Y. Tokura, Phys. Rev. Lett. **83**, 4872 (1999).

⁷C.H. Chen, S-W. Cheong, and H.Y. Hwang, J. Appl. Phys. **81**, 4326 (1997).

⁸S.W. Cheong and H. Y. Hwang, in *Colossal Magnetoresistance*

Oxides, edited by Y. Tokura (Gordon and Breach, New York, 1999).

⁹F. Damay, C. Martin, A. Maignan, and B. Raveau, J. Magn. Mater. **183**, 143 (1998).

¹⁰J.B. Goodenough, Phys. Rev. **100**, 564 (1955).

¹¹J. Rodríguez-Carvajal, M. Hennion, F. Moussa, A.H. Moudden, L. Pinsard, and A. Revcolevschi, Phys. Rev. B **57**, R3189 (1998).

¹²P.G. Radaelli, D.E. Cox, M. Marezio, S-W. Cheong, P.E. Schiffer, and A.P. Ramirez, Phys. Rev. Lett. **75**, 4488 (1995).

¹³I.S. Elfimov, V.I. Anisimov, and G.A. Sawatzky, Phys. Rev. Lett. **82**, 4264 (1999).

¹⁴M. Benfatto, Y. Joly, and C.R. Natoli, Phys. Rev. Lett. **83**, 636 (1999).

¹⁵S. Ishihara and S. Maekawa, Phys. Rev. Lett. **80**, 3799 (1998).

¹⁶J.P. Hannon, G.T. Trammel, M. Blume, and D. Gibbs, Phys. Rev. Lett. **61**, 1245 (1988).

¹⁷M. Abbate, F.M.F. de Groot, J.C. Fuggle, A. Fujimori, O. Strelbel, F. Lopez, M. Domke, G. Kaindl, G.A. Sawatzky, M. Takano, Y. Takeda, H. Eisaki, and S. Uchida, Phys. Rev. B **46**, 4511 (1992).

¹⁸E. Pellegrin *et al.* (private communication).